文章编号 2095-1531(2019)04-0791-13

Error analysis and fabrication of low-stepped mirrors

ZHANG Min[1,2], LV Jin-guang[1], LIANG Jing-qiu[1*], LIANG Zhong-zhu[1*], QIN Yu-xin[1], WANG Wei-biao[1]

(1. *State Key Laboratory of Applied Optics, Changchun Institute of Optics, Fine Mechanics and Physics, Chinese Academy of Sciences, Changchun* 130033;
2. *University of Chinese Academy of Sciences, Beijing* 100049)

* *Corresponding author, E-mail: liangjq@ciomp.ac.cn; liangzz@ciomp.ac.cn*

Abstract: In this study, a static and light Fourier transform infrared spectrometer based on stepped mirrors and a grid beam splitter was proposed. By introducing two stepped mirrors into the interference system, the optical path difference is discretized and the 2-dimensional sampling of the interferogram is obtained. Furthermore, by introducing the grid beam splitter into the interference system, the volume and weight are decreased. Stepped mirrors as the core optical devices of such a spectrometer, its step height consistency, face flatness and the structure's precision determine the spectral sampling interval, resolution and noise of the system. We propose a method based on MOEMS technology involving multiple depositions accompanied by a 50% reduction in thickness at every iteration to fabricate a low-stepped mirror with 32 steps and 0.625 μm in step height. The test results show that the root-mean-square of roughness is 1.72 nm and that the average height of the real steps is 626.9 nm. The effect of the height error on the recovered spectrum is analyzed. In order to reduce the influence of this error, two methods are proposed: one is through using tooling factor to reduce the monitoring error of the film thickness, thus reducing the height error; the other is through using the least-squares approximation cosine polynomial algorithm to correct the recovered spectrum. The spectrum-constructing error(SCE) is reduced to 2.34%, which meets the requirements of spectral restoration. Finally, the experiment was carried out using low stepped mirrors and the interferograms were obtained before and after the addition of the sample. The absorption spectrum of the sample acetonitrile can be obtained using a Fourier transform.

Key words: fourier transform infrared spectrometer; low stepped multi-level mirror; height error analysis

收稿日期:2018-02-05;**修订日期**:2018-03-05

基金项目:国家自然科学基金(No. 61627819, No. 61575193, No. 61805239, No. 61727818, No. 61735018);吉林省科技发展计划(No. 20190303063SF, No. 20180201024GX, No. 20150520101JH, No. 20170204077GX);中国科学院创新促进会基金(No. 2018254);吉林省中青年科技创新团队项目(No. 20190101012JH)

Supported by National Natural Science Foundation of China(No. 61627819, No. 61575193, No. 61805239, No. 61727818, No. 61735018); Scientific and Technological Development Project of Jilin Province (No. 20190303063SF, No. 20180201024GX, No. 20150520101JH, No. 20170204077GX); Youth Innovation Promotion Association of the Chinese Academy of Sciences(No. 2018254); Leading Talents and Team Project of Scientific and Technological Innovation for Young and Middle-aged Groups in Jilin Province(No. 20190101012JH)

低阶梯多级微反射镜高度误差分析及制作研究

张　敏[1,2],吕金光,梁静秋[1*],梁中翥[1*],秦余欣[1],王维彪[1]
(1. 中国科学院 长春光学精密机械与物理研究所 应用光学国家重点实验室,吉林 长春 130033;
2. 中国科学院大学,北京 100049)

摘要:本文提出了一种基于多级微反射镜和栅格分束器的静态轻型傅立叶红外变换光谱仪,通过两个多级微反射镜实现光程差的空间离散和干涉图的静态二维采样,通过引入栅格分束器有效降低了系统的体积和重量。作为该光谱仪的核心光学器件,多级微反射镜的阶梯高度一致性、面型平整度和结构精度是决定采样间隔、分辨率和噪声等仪器指标的主要因素。本文提出了基于 MOEMS 技术的厚度依次减半多层膜法,制作了台阶高度为 0.625 μm,阶梯数为 32 的低阶梯多级微反射镜。测得实际阶梯高度平均值为 626.9 nm,表面粗糙度均方根值为 1.72 nm。分析了阶梯高度误差对光谱复原的影响,提出了两种阶梯高度误差校正方法,分别为通过修正因子来减小膜厚监控误差,和利用最小二乘余弦多项式算法对复原光谱进行校正。校正后的复原光谱误差(SCE)降低为 2.34%,满足系统对光谱复原的要求。最后,将该低阶梯多级微反射镜置入光谱仪中,得到乙腈样品的干涉图和复原光谱图。

关　键　词:傅立叶变换红外光谱仪;低阶梯多级微反射镜;高度误差分析
中图分类号:TN214;O438.2;TN305.8　　**文献标识码:**A　　doi:10.3788/CO.20191204.0791

1　Introduction

An infrared spectrometer is an instrument that uses the absorption characteristics of different wavelengths of infrared radiation to analyze the molecular structure and chemical composition[1-3]. It can perform high-precision spectral measurements on substances and conduct qualitative or quantitative analysis on them. It has a wide range of applications in reconnaissance, resource exploration, medical treatment, environmental monitoring and chemical analysis[4-8]. In recent years, with the strengthening of detection requirements and demand for real-time monitoring, infrared spectrometers are gradually developing for high precision, miniaturization and weight reduction. Fourier transform infrared spectrometers (FTIR) have the advantages of having multiple channels, large radiant fluxes, low stray light, accurate wave numbers and high precision. This allows them to achieve high-resolution detection and analysis of weak radiators. Therefore, they have undergone extensive research[9-12]. FTIRs are classified into two types: the time modulation type and the spatial modulation type. These classification depend on the way in which the optical path difference is generated. The time-modulated FTIR generates time-series interferograms by moving mirror scanning or by other methods[13-14] and the spatially modulated FTIR generates interferograms of spatial sequences through different spatial positions[15-17]. Since the currently most widely used time-modulated FTIR contains movable parts, the environmental requirements are relatively strict and the interference signal is easily disturbed by vibrations. Therefore, in recent years, the miniaturized and lightweight spatial modulation type FTIR has been studied extensively.

This research group proposes a lightweight static spatial modulation FTIR that uses micro-optical electromechanical system technology. The technology utilizes two orthogonally placed high- and low-step multi-level micromirrors to achieve spatially continuous sampling of optical path differences[18]. The high- and low-step multi-level micromirrors are the core components of the FTIR. The structure is sub-micron level in height with a large lateral area and high structural precision. Due to the step height consistency, surface flatness and structural accuracy of the low-step multi-level micro-mirrors, the spectral sampling interval, resolution and noise are directly affected. Even when the error is too large, the interferogram is reversed. Therefore, the spectral recovery is affected, and the precision fabrication and error analysis of the device are of great significance. This research group successfully produced a high-step multi-level micro-mirror with a step height of 20 μm for 32 steps using the bevel lamination method[19]. Since the step height of the low-step multi-level micromirror is 0.625 μm, it is difficult to achieve the required device accuracy using conventional processing methods. In this paper, the "method of thickness reduction of half-multilayer films" is proposed, which uses the coating technology to precisely control the accuracy, consistency and uniformity of the step height. Low-step multi-level micro-mirrors were tested and the errors and their causes were analyzed and discussed. A spectrogram of the acetonitrile sample was obtained experimentally.

2 Working Principles

Fig. 1 is a schematic structural diagram of the proposed static and light Fourier transform infrared spectrometer that uses a multi-stage micromirror and a grid beam splitter. As shown in Fig. 1, the spectrometer system is mainly composed of an infrared light source, a collimation system, a sample cell, a grid beam splitter, a high- and low-step multi-level micro-mirror, a beam reduction system and a medium-wave infrared area array detector. The working principle is as follows: the light emitted by the light source passes through the collimating system and becomes a parallel beam. The beam passes through the sample pool and reaches the grid beam splitter, wherein the light beam incident on the grating edge is absorbed by the absorption film and meets the grid. The beam is split by the beam splitting film into two beams of coherent light that reach the high and low step multi-level micromirrors. The optical path difference of the beam is sampled by high- and low-step multi-level micromirrors. After the beam is reflected by the high- and low-step multi-stage micro-mirrors, it returns to the grid beam splitter and interferes. After being reduced by the beam-shrinking system, it is received by the infrared detector to obtain an interferogram. The two interferograms obtained before and after the sample is added are image processed and then subjected to Fourier transformation to obtain a restored spectrum.

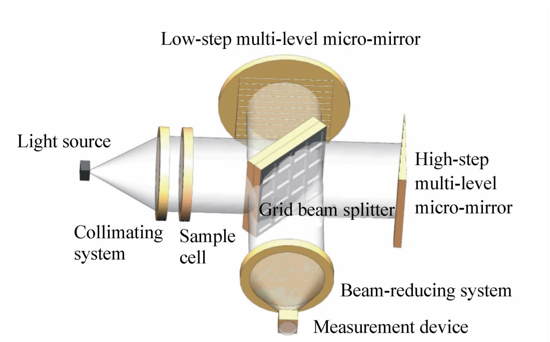

Fig. 1　Schematic diagram of the static and light FTIR

图 1　静态轻型 FTIR 结构示意图

As the core device of FTIR, the high and low step multi-level micromirrors have the same step series, step width and step length but different step height. The sum of the step heights of the low-step multi-level micromirrors is equal to the single step height of the high-step multi-stage micromirrors. The number of sampling points N of the spectrometer follows the Nyquist-Shanno sampling theorem. In other words, the sampling interval Δ is less than or equal to one half of the minimum wavelength. The operating band of this system is 3.7 – 4.8 μm. We choose the step height of the low-step multi-level micro-mirror to be 0.625 μm, then choose 1 024 sampling points and 32 high and low steps. The structure of the low-step multi-level micro-mirror is as shown in Fig. 2. The step width is W, the step length is L and the sub-step height is H. Each localized interferogram function can be expressed as

$$I(l,m) = \int_0^\infty B(\nu)\exp[\mathrm{j}2\pi\nu\delta(l,m)]\mathrm{d}\nu \ ,(1)$$

where l and m represent the number of steps in the two multi-level micromirrors, $I(l,m)$ represents the intensity of the interferogram at the spatial sampling point (l,m), $B(\nu)$ is the power spectral density of the optical signal, ν is the spatial frequency of the optical signal, $\delta(l,m)$ is the optical path difference at the spatial sampling point (l,m). A restoration spectrum can be obtained by performing Fourier transform on the equation (1).

$$B(\nu) = \sum_{l=1}^{32}\sum_{m=1}^{32} I(l,m)\exp[\mathrm{j}2\pi\nu\delta(l,m)] \ . \qquad (2)$$

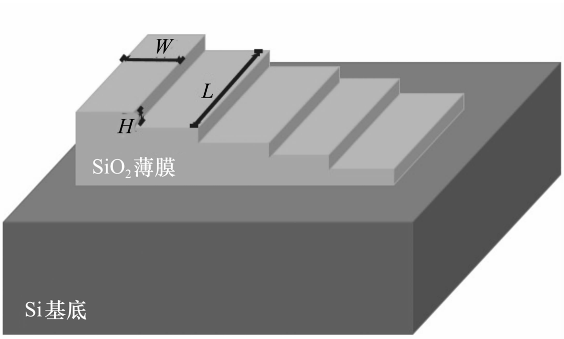

Fig. 2 Schematic diagram of low-step multi-level micro-mirrors

图 2 低阶梯多级微反射镜结构示意图

3 Step Height Error Analysis of Low-step Multi-level Micro-mirrors

Thickness error introduced during the fabrication of low-step multi-level micromirrors can lead to height errors in the sub-steps, resulting in loss from spectral distortion and decreased spectral performance. The influence of height error on spectral recovery, therefore, needs to be analyzed. It is assumed that the high-step multi-stage micromirrors are in an ideal state. That is, all sub-step heights are 20 μm. The additional optical path difference caused by the m-th sub-step height error of the low-step multi-stage micromirror is $\Delta\delta(m)$, and the intensity distribution of the interferogram actually detected on the receiving plane is obtained by (1)

$$I'(l,m) = \int_0^\infty B(\nu)\exp\{\mathrm{j}2\pi\nu[\delta(m) + \Delta\delta(m)]\}\mathrm{d}\nu \ . \qquad (3)$$

Let the height deviation of the low-step mth-order sub-step be $H(m)$ and the resulting optical path difference be

$$\delta'(l,m) = 2(Nm - l)H + 2H(m) \ . \qquad (4)$$

Substituting (3) there is

$$I'(l,m) = \int_0^\infty B(\nu)\exp\{\mathrm{j}2\pi\nu[2(Nm - l)H + 2H(m)]\}\mathrm{d}\nu \ . \qquad (5)$$

The discrete Fourier transform (DFT) of (5) can restore the spectral information of the incident light signal.

$$B'(\nu) = \sum_{l=1}^{32}\sum_{m=1}^{32} I'(l,m)\exp[\mathrm{j}2\pi\nu\delta(l,m)] \ . \qquad (6)$$

Defining the Spectrum-Constructing Error (SCE) as the spectral evaluation function, SCE can be expressed as:

$$SCE = \frac{\sum_{k=0}^{N^2-1} | B'[v(k)] - B[v(k)] |}{\sum_{k=0}^{N^2-1} B[v(k)]} \ , \qquad (7)$$

where $B'[v(k)]$ represents the actual recovered spectrum with errors and $B[v(k)]$ represents the ideal spectrum. The Monte Carlo method is used to analyze the sub-step height error. Assuming that the 32 step heights follow a normal distribution with an average of 0.625 μm, the number of sampling points is 1 000 and the height standard deviation is σ. The corresponding 32 step heights will result in 32 random number sequences $G(i,m)$, of which $i = 1,2,3 \cdots 1\ 000$. The additional optical path difference expression at the i sampling points of the m-th sub-step is

$$\Delta\delta_i(m) = 2H(i,m) . \quad (8)$$

For each sample point i, a sample inversion spectral sequence $B_i(k)$ with a height error is obtained. After averaging the inversion spectrum sequence, a relationship between the SCE value and the step height standard deviation is produced, as shown in Fig. 3. It can be seen from the figure that the SCE value increases monotonically with the standard deviation of the step height, showing a linear relationship. Therefore, in the manufacturing process of the multi-level micromirror, the height standard deviation range of a multi-level micromirror can be obtained according to the requirement of the SCE value. In this system, when SCE$\leqslant$0.01 is required, the standard deviation of the step height should satisfy $\sigma \leqslant 5$ nm.

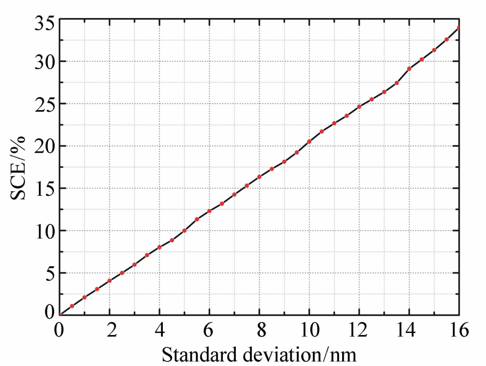

Fig. 3　SCE varies with height standard deviation σ of the sub-mirror

图 3　光谱评价函数 SCE 随阶梯高度标准差 σ 变化曲线

4　Production, Testing and Analysis of Low-step Multi-level Micro-mirrors

The low-step multi-level micromirror was fabricated by sequentially reducing the thickness using the multilayer film method. A double-sided polished single crystal silicon wafer with a thickness of 5 mm, a diameter of 70 mm and a surface roughness of 0.2 nm was used as a substrate.

The manufacturing process is shown in Fig. 4.

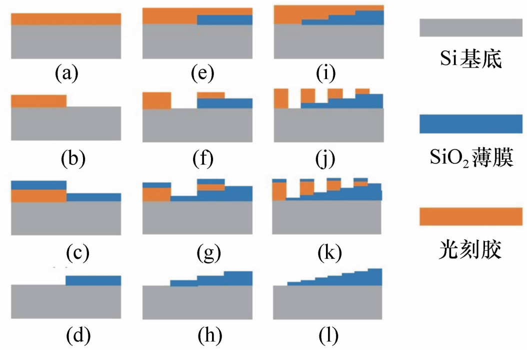

Fig. 4　Flow diagram of low-stepped multi-level micromirrors (with 8 steps as an example)

图 4　低阶梯多级微反射镜制备流程图(以 8 台阶为例)

The specific steps are: (a) spin-coat AZ4620 photoresist on the surface of the single crystal silicon wafer (Fig. 4(a)); (b) obtain a mask pattern in a specific area of the substrate by using exposure and development (Fig. 4(b)); (c) selecting a SiO_2 target with a purity of 99.99% and depositing a SiO_2 film with a thickness of 10 μm by electron beam evaporation (Fig. 4(c)); (d) use a stripping process to obtain a stepped structure (Fig. 4(d)). By repeating the above fabrication steps, a low-step multi-stage micromirror with a number of steps of 32 and a sub-step height of 0.625 μm is produced, in which the film thickness was gradually halved as the number of coatings increased. Finally, 150 nm Au was vapor-deposited as a high-reflection film to complete the fabrication of the low-step multi-stage micromirror. Fig. 5 is a photograph of a low-step multi-level mi-

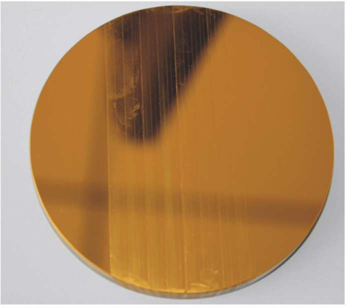

Fig. 5　Low-step multi-level micro-mirrors

图 5　低阶梯多级微反射镜照片

cromirror and Fig. 6 is a partially enlarged view.

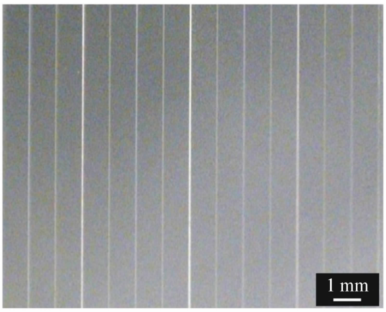

Fig. 6 Local detail of the low-step multi-level micro-mirrors

图 6 局部低阶梯多级微反射镜放大图

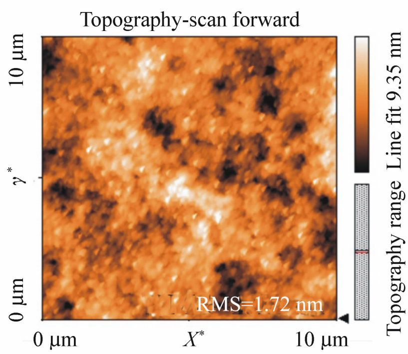

Fig. 7 Roughness test chart of low-step multi-level mi-cro-mirrors

图 7 低阶梯多级微反射镜粗糙度测试图

The roughness of the low-step multi-level micro-mirror was tested by a Swiss Nanosurf Core AFM. The measured RMS value was 1.72 nm, as shown in Fig. 7, which satisfies the system requirements for the surface of the step mirror. KLA-Tencor P-16 + steps were used. The instrument measures the step height of the low-step multi-level micro-mirror with a scanning speed of 100 μm/s and a scanning frequency of 100 Hz. The test results are shown in Fig. 8. After averaging the points on each step, the steps were successively subtracted to obtain the step height of the 32-stage multi-level micromirror. Fig. 9 shows the difference between the actual step height and the theoretical step height. The step test height of the low-step multi-stage micromirror was counted, and the results are shown in Tab. 1.

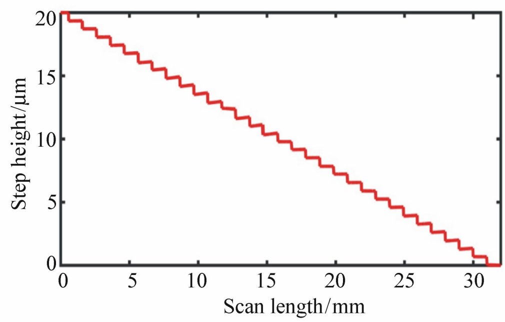

Fig. 8 Step height test results of low stepped micromirror with 32 steps

图 8 32 级低阶梯多级微反射镜台阶高度测试图

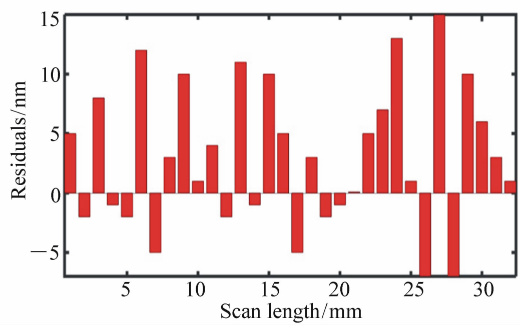

Fig. 9 Step height difference between the measured values and their theoretical values

图 9 台阶高度测试值与理论值差值图

Tab. 1 Statistical test results of step height

表 1 台阶高度测试结果统计表

Step Height	Value
Maximum value/ Highest positive deviation	640/15
Minimum value/Lowest negative value	618/ −7
Average value/Average deviation	626.9/1.9
Standard deviation	7.4

Due to the limitations of the film thickness controller and the complexity of multiple coatings, the standard deviation of the measured step height is 7.4 nm and the height average is 626.9 nm, which is 1.9 nm higher than the average of the ideal step height. As can be seen from Fig. 3, the SCE at this time was 15.02%.

With regards to the reason behind the error in step height, it is believed that there is some deviation between the film thickness of the quartz crystal film thickness controller and the film thickness of the substrate evaporated during the coating process.

There are actually two main sources of deviation. The first is that the distance from the evaporation source to the crystal plate and the substrate is not equal, resulting in different amounts of evaporating particles simultaneously reaching the crystal plate and the substrate. The second is the crystal plate and the substrate, whose materials and surface properties are different, resulting in different film growth rates. Since the fabrication of the device structure requires 5 coats, the final error is the compound of multiple error accumulation.

The film thickness monitoring error can be reduced by determining the tooling factor [20].

This is expressed as TF and has the following calculation:

$$TF(100\%) = \frac{D_s}{D_q} \times 100\% , \qquad (9)$$

where D_s is the thickness of the base film layer and D_q is the measurement thickness of the crystal plate. Through multiple coating experiments, a number of TF values were obtained and averaged to obtain a correction factor of 112% for SiO_2.

The sampling error was corrected by an algorithm. In this paper, the least squares cosine fitting algorithm (LSC) using cosine polynomials[21] was used to correct the non-uniformity sampling of the prepared low-step multi-level micro-mirror steps.

The spectrum under a continuous light source was analyzed. Fig. 10 and Fig. 11 respectively show the restored spectra obtained by Fourier transform (FFT) and LSC algorithm, wherein the red curve (2) represents the actual spectral curve including height error, and the blue curve (1) represents the ideal spectral curve with a height error of zero. It can be clearly seen from Fig. 10 and Fig. 11 that the actual spectrum recovered by FFT has a relatively large amount of noise and therefore cannot meet the system requirements for spectrum recovery. The spectrum restored by the LSC algorithm was better than the ideal spectrum. Its spectral error factor SCE at this time was only 2.34%. Within a reasonable range, the accuracy of the restored spectrum can be guaranteed.

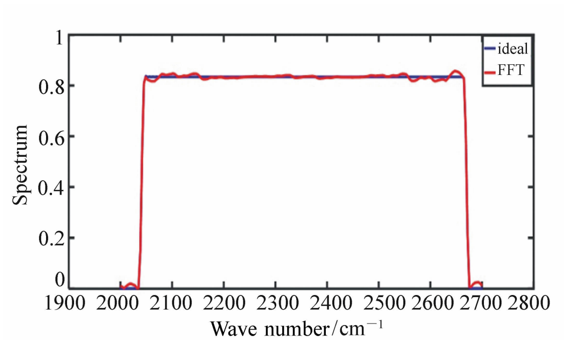

Fig. 10　Comparison of the ideal spectrum and the actual spectrum using the FFT algorithm with height error

图 10　使用 FFT 算法时高度误差影响下的实际光谱和理想复原光谱对比图

5　Spectral Measurement Experiment

The produced high-precision low-step multi-stage micromirror was placed in an optical system for the experiment. Fig. 12 is a schematic diagram of the static light-space modulation FTIR principle. The SiC infrared light source was used and the step height of the high-step multi-stage micro-mirror was 20 μm with 32 steps. The detector selects the HgCdTe medium-wave infrared array CCD with a resolution of 320 × 256 pixels, each being 30 μm × 30 μm. The beam splitter and compensator plate act

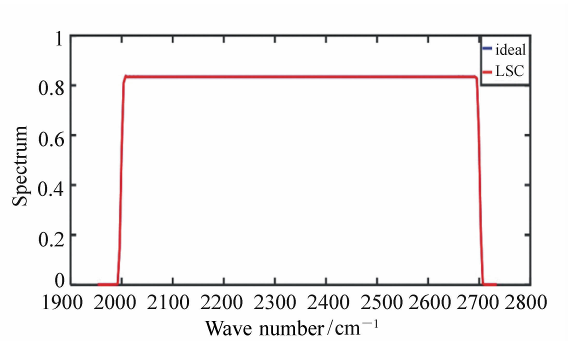

Fig. 11 Comparison of the ideal spectrum and the actual spectrum using the LSC algorithm with height error

图 11 使用 LSC 算法时高度误差影响下的实际光谱和理想复原光谱对比图

as beam splitters, where the number of grids is 20 × 20 and the grid size is 1 990 μm × 2 818 μm. The collimation system consists of two ZnSe lenses and one CaF_2 lens. The constricting system consists of two Si lenses and five Ge lenses.

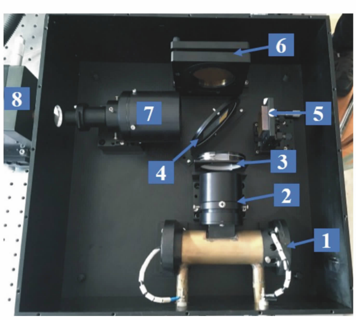

Fig. 12 Static spatial modulation FTIR prototype. 1 light source; 2 collimating system; 3 sample chamber; 4 beam splitter and compensation plate; 5 high-stepped micromirror; 6 low-stepped micromirror; 7. constricting system; 8 infrared detector array

图 12 静态空间调制 FTIR 原理样机. 1 光源;2 准直系统;3 样品池;4 栅格分束板和栅格补偿板;5 高阶梯多级微反射镜;6 低阶梯多级微反射镜;7 缩束系统;8 红外探测器

Spectral measurements were taken from samples of acetonitrile. The interferograms before and after the injection of the acetonitrile solution were separately collected, as shown in Fig. 13(a) and (b). After subtracting the two from each other, a Fourier transform is performed to obtain the absorption spectrum of the sample[22], as shown in Fig. 14.

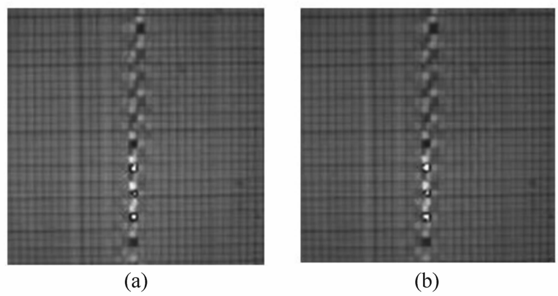

Fig. 13 Interferogram (a) without the sample; (b) with the sample

图 13 干涉图(a)加入样品前;(b)加入样品后

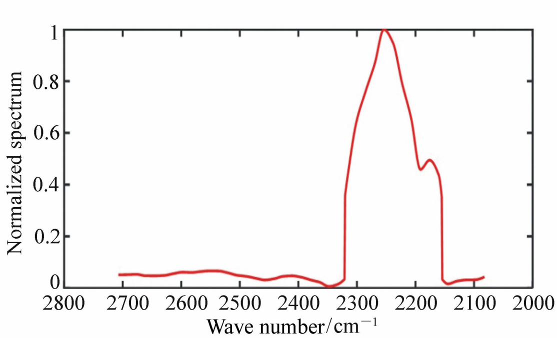

Fig. 14 Recovered spectrum of acetonitrile

图 14 乙腈样品的复原光谱曲线

6 Conclusion

Fabrication and error analysis were performed on the Low-step multi-level micromirrors of the core devices in a spatially modulated FTIR. A 32-stage low-step multi-stage micromirror was fabricated by sequentially reducing the thickness by half using the multilayer film method. The test results showed that the step height averaged 626.9 nm with a standard deviation of 7.4 nm. The influence of height error on the restored spectrum was analyzed and two error correction methods were proposed. The film thickness monitoring error can be reduced by introducing a correction factor in the coating process; by using the LSC algorithm to correct the non-uniformity of

the spectral sampling, the SCE of the actual recovered spectrum is reduced from 15.02% to 2.34%, which satisfies the step-height requirements of the system. Using the high-precision low-step multi-stage micro-mirror produced in this paper, the spectrum of an acetonitrile sample was obtained, which showed that the low-step multi-level micro-mirror fabricated by this method can meet the performance requirements of the system.

——中文对照版——

1 引 言

红外光谱仪是利用物质对不同波长红外辐射的吸收特性,进行分子结构和化学组成分析的仪器[1-3],可对物质进行高精度的光谱测量,并对其进行定性或定量分析,在军事侦察、资源勘探、医学治疗、环境监测、化学分析等领域有着广泛的应用[4-8]。近年来,随着检测要求的提高和实时监测的需求,红外光谱仪逐渐向着高精度、微型化和轻量化的方向发展。傅立叶变换红外光谱仪(Fourier Transform Infrared Spectrometer, FTIR)具有多通道、辐射通量大、杂散光低、波数准确、精度高等优点,可实现对弱辐射体的高分辨率探测和分析,因此得到了广泛的研究[9-12]。根据光程差产生方式的不同,FTIR 可分为时间调制型和空间调制型两类。时间调制型 FTIR 通过动镜扫描或其他方式产生时间序列干涉图[13-14],空间调制型 FTIR 则通过不同的空间位置产生空间序列的干涉图[15-17]。由于目前普遍应用的时间调制型 FTIR 内部含有可动部件,因此对环境要求比较严格,易因震动而导致干涉信号失真。因此微型化、轻量化的空间调制型 FTIR 在近几年得到广泛的研究。

本课组提出了一种基于微光机电系统技术的轻量化静态空间调制型 FTIR。它利用两个正交放置的高、低阶梯多级微反射镜,实现光程差的空间连续采样[18]。高、低阶梯多级微反射镜是 FTIR 的核心器件,其结构高度在亚微米量级,横向面积大,且结构精度要求高。由于低阶梯多级微反射镜的阶梯高度一致性、面型平整度和结构精度直接影响了光谱采样间隔、分辨率和噪声,甚至当误差过大时,会导致干涉图发生反转,从而影响光谱复原,因此该器件的制作精度以及误差分析具有十分重要的意义。本课题组采用斜面叠片法成功制作出了阶梯高度为 20 μm,阶梯数为 32 的高阶梯多级微反射镜[19]。由于低阶梯多级微反射镜阶梯高度为 0.625 μm,传统的加工方法难以达到器件精度要求。本文提出采用“厚度依次减半多层膜法”,利用镀膜技术,精确控制阶梯高度的准确性、一致性和均匀性。对所制作低阶梯多级微反射镜进行了测试,对产生误差的原因及误差对光谱复原的影响进行了分析和讨论。通过实验得到了乙腈样品的光谱图。

2 工作原理

图 1 为本文提出的基于多级微反射镜和栅格分束器的静态轻型傅立叶变换红外光谱仪的结构示意图。如图 1 所示,光谱仪系统主要由红外光源,准直系统,样品池,栅格分束器,高、低阶梯多级微反射镜,缩束系统和中波红外面阵探测器组成。其工作原理如下:由光源发出的光经过准直系统后变成平行光束,该光束经过样品池后到达栅格分束器,其中入射到栅棱的光束被吸收膜吸收,入射到栅格内的光束被分束膜分成两束相干光分别到达高、低阶梯多级微反射镜。由高、低阶梯多级微反射镜对光束的光程差进行空间离散采样。光束由高、低阶梯多级微反射镜反射后,返回栅格分束器并发生干涉,再经缩束系统缩束后,被红外探测器接收得到干涉图,将加入样品前和加入样品后的两幅干涉图进行图像处理,再经过傅立叶变换即可得到复原光谱。

作为 FTIR 的核心器件,高、低阶梯多级微反

射镜具有相同的阶梯级数、阶梯宽度、阶梯长度及不同的阶梯高度。低阶梯多级微反射镜的阶梯高度总和等于高阶梯多级微反射镜的单个阶梯高度。光谱仪的采样点数 N 遵循 Nyquist-Shanno 采样定理,即采样间隔 Δ 要小于等于最小波长的二分之一。本系统的工作波段为 3.7 ~ 4.8 μm,低阶梯多级微反射镜的台阶高度为 0.625 μm,采样点数为 1 024,高、低阶梯的阶梯级数均为 32。低阶梯多级微反射镜结构如图 2 所示,阶梯宽度为 W,阶梯长度为 L,子阶梯高度为 H。各个定域的干涉图函数可以表示为

$$I(l,m) = \int_0^{\infty} B(\nu)\exp[\mathrm{j}2\pi\nu\delta(l,m)]\mathrm{d}\nu \ , \quad (1)$$

式中:l 和 m 分别表示高低两个多级微反射镜的阶梯数,$I(l,m)$ 表示空间采样点 (l,m) 处的干涉图强度,$B(\nu)$ 为光信号的功率谱密度,ν 为光信号的空间频率,$\delta(l,m)$ 为空间采样点 (l,m) 处的光程差。对式(1)进行傅立叶变换即可得到复原光谱。

$$B(\nu) = \sum_{l=1}^{32}\sum_{m=1}^{32} I(l,m)\exp[\mathrm{j}2\pi\nu\delta(l,m)] \ . \quad (2)$$

3 低阶梯多级微反射镜台阶高度误差分析

在低阶梯多级微反射镜的制作过程中引入的厚度误差会导致子阶梯出现高度误差,使复原光谱失真及光谱性能下降。因此需分析高度误差对光谱复原的影响。

假设高阶梯多级微反射镜处于理想状态,即所有子阶梯高度均为 20 μm。设低阶梯多级微反射镜第 m 阶子阶梯高度误差引起的附加光程差为 $\Delta\delta(m)$,由(1)式可得接收平面上实际探测到的干涉图光强分布为

$$I'(l,m) = \int_0^{\infty} B(\nu)\exp\{\mathrm{j}2\pi\nu[\delta(m) + \Delta\delta(m)]\}\mathrm{d}\nu \ , \quad (3)$$

设第 m 阶低阶梯子阶梯的高度偏差为 $H(m)$,则引起的光程差为

$$\delta'(l,m) = 2(Nm - l)H + 2H(m) \ , \quad (4)$$

代入式(3)可得

$$I'(l,m) = \int_0^{\infty} B(\nu)\exp\{\mathrm{j}2\pi\nu[2(Nm - l)H + 2H(m)]\}\mathrm{d}\nu \ , \quad (5)$$

对式(5)进行离散傅立叶变换(DFT)即可还原出入射光信号的光谱信息

$$B'(\nu) = \sum_{l=1}^{32}\sum_{m=1}^{32} I'(l,m)\exp[\mathrm{j}2\pi\nu\delta(l,m)] \ . \quad (6)$$

定义光谱复原误差(Spectrum-Constructing Error)为光谱评价函数,用 SCE 表示:

$$SCE = \frac{\sum_{k=0}^{N^2-1} | B'[v(k)] - B[v(k)] |}{\sum_{k=0}^{N^2-1} B[v(k)]} \ , \quad (7)$$

其中:$B'[v(k)]$ 表示含有误差时的实际复原光谱,$B[v(k)]$ 表示理想光谱。采用 Monte Carlo 方法对子阶梯高度误差进行分析,假设 32 个阶梯高度服从正态分布,平均值为 0.625 μm,采样点数为 1 000,高度标准差为 σ,则对应 32 个阶梯高度将产生 32 个随机数序列 $G(i,m)$,其中 $i = 1,2,3 \cdots 1\ 000$。第 m 个子阶梯的 i 个采样点处的附加光程差表达式为

$$\Delta\delta_i(m) = 2H(i,m) \ . \quad (8)$$

对每一个采样点 i,都能得到存在高度误差的采样反演光谱序列 $B_i(k)$。将反演光谱序列取平均值后,得到 SCE 值与台阶高度标准差的关系曲线,如图 3 所示。从图可以看出,SCE 值随阶梯高度标准差单调递增,呈现线性关系。因此在多级微反射镜的制作过程中,可以根据 SCE 值的要求,得到多级微反射镜的高度标准差范围。在本系统中,当要求 SCE≤0.01 时,阶梯高度标准差应满足 $\sigma \leqslant 5$ nm。

4 低阶梯多级微反射镜的制作、测试及分析

利用厚度依次减半多层膜法制作低阶梯多级微反射镜。实验采用厚度为 5 mm,直径为 70 mm,表面粗糙度为 0.2 nm 的双面抛光单晶硅片作为基片。

制作工艺流程如图 4 所示,具体步骤如下:(a)在单晶硅片表面旋涂 AZ4620 光刻胶(图 4

(a));(b)通过曝光、显影,在基片特定区域得到掩膜图形(图 4(b));(c)选择纯度为 99.99% 的 SiO_2靶材,通过电子束蒸发沉积厚度为 10 μm 的 SiO_2薄膜 (图 4(c));(d)通过剥离工艺得到台阶结构(图 4(d))。重复以上制作步骤,通过 5 次光刻-镀膜,制作出台阶数为 32,子阶梯高度为 0.625 μm 的低阶梯多级微反射镜,其中薄膜厚度随镀膜次数的增加逐渐减半。最后,蒸镀 150 nm Au 作为高反膜,完成低阶梯多级微反射镜的制作。图 5 为低阶梯多级微反射镜照片,图 6 为局部放大图。

采用瑞士 Nanosurf Core AFM 对低阶梯多级微反射镜进行粗糙度测试,测得 RMS 值为 1.72 nm,如图 7 所示,满足系统对阶梯镜表面的要求,采用 KLA-Tencor P-16 + 台阶仪对低阶梯多级微反射镜的台阶高度进行测量,扫描速度为 100 μm/s,扫描频率为 100 Hz,测试结果如图 8 所示。将每一级阶梯上的点求取平均值后,依次相减得到 32 级多级微反射镜的台阶高度。图 9 为实际阶梯高度与理论阶梯高度的差值。对低阶梯多级微反射镜的台阶测试高度进行统计,结果如表 1 所示。

由于膜厚控制仪的局限性及多次镀膜的复杂性,实测台阶高度的标准差为 7.4 nm,高度平均值为 626.9 nm,比理想台阶高度平均值高 1.9 nm。根据图 3 可知,此时的 SCE 为 15.02%。

对阶梯高度误差产生的原因进行分析,认为镀膜过程中石英晶体膜厚控制仪显示的膜厚与基片蒸镀的膜厚存在一定的偏差。偏差来源主要有两个,第一是蒸发源到晶振片及基片的距离不相等,从而导致在相同的时间内到达晶振片和基片的蒸发粒子数量不同;第二是晶振片和基片的材料及表面性质不同,导致各自的薄膜生长速率不同。由于器件结构的制作需要 5 次镀膜,最终的误差为多次累积的结果。

可通过确定修正因子(Tooling Factor)减小膜厚监控误差[20]。修正因子用 TF 表示,其表达式如下:

$$TF(100\%) = \frac{D_s}{D_q} \times 100\% \quad , \qquad (9)$$

其中 D_s是基底膜层厚度,D_q是晶振片测试厚度。通过多次镀膜实验,求得多个 TF 值,对其取平均,即可得到 SiO_2的修正因子为 112%。

此外,还通过算法对采样误差进行校正。本文采用的是基于余弦多项式的最小二乘余弦拟合算法(LSC)[21],对所制备的低阶梯多级微反射镜阶梯的非均匀性采样进行了误差校正。

对连续光源下的光谱进行分析,图 10 和图 11分别表示利用傅立叶变换(FFT)和 LSC 算法得到的复原光谱,其中红色曲线(2)代表含有高度误差时的实际光谱曲线,蓝色曲线(1)代表高度误差为零时的理想光谱曲线。由图 10 和 11 可以明显看出,利用 FFT 复原的实际光谱,噪声比较大,不能满足系统对复原光谱的要求。而利用 LSC 算法复原的光谱,则与理想光谱重合的比较好,并且此时的光谱误差因子 SCE 仅为 2.34%,在合理范围内,可以保证复原光谱的准确性。

5　光谱测量实验

将制作的高精度低阶梯多级微反射镜放入光学系统进行实验,图 12 为静态轻型空间调制 FT-IR 原理样机图。采用 SiC 红外光源,高阶梯多级微反射镜台阶高度为 20 μm,阶梯数为 32。探测器选取碲镉汞(HgCdTe)中波红外面阵 CCD,像素单元数为 320 × 256,单个像元尺寸为 30 μm × 30 μm。分束器和补偿板为栅格分束器,其中栅格数为 20 × 20,栅格尺寸为 1 990 μm × 2 818 μm。准直系统由两片 ZnSe 透镜和一片 CaF_2透镜组成,缩束系统由两片 Si 透镜和五片 Ge 透镜组成。

对乙腈样品进行光谱测量。分别采集注入乙腈溶液前后的干涉图,如图 13(a)和 13(b)所示。二者相减之后进行傅立叶变换即可得到样品的吸收光谱[22],如图 14 所示。

6　结　论

对空间调制 FTIR 中的核心器件低阶梯多级微反射镜进行了制作和误差分析。采用厚度依次减半多层膜法对 32 级低阶梯多级微反射镜进行

了制作，测试结果显示，阶梯高度平均值为626.9 nm，标准差为7.4 nm。分析了高度误差对复原光谱的影响，提出两种误差校正方法。可以通过在镀膜过程中引入修正因子，减少膜厚监控误差；通过采用LSC算法对光谱采样的非均匀性进行校正，使实际复原光谱的SCE由15.02%降为2.34%，满足系统对阶梯高度的要求。利用本文制作的高精度低阶梯多级微反射镜进行实验，得到了乙腈样品的光谱图，表明运用该方法制作的低阶梯多级微反射镜可满足系统性能需求。

参考文献：

[1] BRACHET F,HÉBERT P J,CANSOT E,*et al.*. Static Fourier transform spectroscopy breadboards for atmospheric chemistry and climate[J]. *Proceedings of SPIE*,2008,7100:710019.

[2] REYES D,SCHILDKRAUT E R,KIM J,*et al.*. A novel method of creating a surface micromachined 3D optical assembly for MEMS-based miniaturized FTIR spectrometers[J]. *Proceedings of SPIE*,2008,6888:68880D.

[3] SIN J,LEE W H,POPA D,*et al.*. Assembled Fourier transform micro-spectrometer[J]. *Proceedings of SPIE*,2006,6019:610904.

[4] 鲍一丹,陈纳,何勇,等.近红外高光谱成像技术快速鉴别国产咖啡豆品种[J].光学 精密工程,2015,23(2):349-355.

BAO Y D,CHEN N,HE Y,*et al.*. Rapid identification of coffee bean variety by near infrared hyperspectral imaging technology[J]. *Opt. Precision Eng.*,2015,23(2):349-355.(in Chinese)

[5] 吴伟平,孙海江.星载紫外环形光谱仪科学数据处理的设计与实现[J].液晶与显示,2017,32(5):387-393.

WU W P,SUN H J. Design and realization of data processing of satellite-borne ultraviolet annular imager[J]. *Chinese Journal of Liquid Crystals and Displays*,2017,32(5):387-393.(in Chinese)

[6] 王岩,杨小虎,王金玲,等.空间遥感光谱仪器光学性能地面检测系统[J].液晶与显示,2017,32(3):206-212.

WANG Y,YANG X H,WANG J L,*et al.*. Ground testing system for detecting optical performance of space remote sensing spectrometer[J]. *Chinese Journal of Liquid Crystals and Displays*,2017,32(3):206-212.(in Chinese)

[7] YAN T Y,ZHANG CH M,LI Q W,*et al.*. Efficient background removal based on two-dimensional notch filtering for polarization interference imaging spectrometers[J]. *Chinese Optics Letters*,2016,14(12):123002.

[8] 欧阳爱国,张宇,程梦杰,等.中红外光谱技术对乙醇汽油乙醇含量的检测[J].中国光学,2017,10(6):752-759.

OUYANG A G,ZHANG Y,CHENG M J,*et al.*. Determination of the content of ethanol in ethanol gasoline using mid-infrared spectroscopy[J]. *Chinese Optics*,2017,10(6):752-759.(in Chinese)

[9] FENG C,WANG B,LIANG ZH ZH,*et al.*. Miniaturization of step mirrors in a static Fourier transform spectrometer: theory and simulation[J]. *Journal of the Optical Society of America B*,2011,28(1):128-133.

[10] 李志刚.真空紫外分波前傅里叶变换光谱技术进展[J].中国光学,2015,8(5):736-743.

LI ZH G. Progress of wavefront-division Fourier transform spectrometry in the vacuum ultraviolet[J]. *Chinese Optics*,2015,8(5):736-743.(in Chinese)

[11] SARDARI B,DAVOLI F,ZCAN M. A broadband configuration for static Fourier transform spectroscopy with bandpass sampling[J]. *Review of Scientific Instruments*,2016,87(10):103106.

[12] 李晚侠,卢启鹏,宋源,等.基于双直角分束器的反射式静态傅里叶光谱仪光学系统[J].光学学报,2017,37(8):0812004.

LI W X,LU Q P,SONG Y,*et al.*. Reflective static Fourier transform spectrometer optical system based on double right-angle beam splitter[J]. *Acta Optica Sinica*,2017,37(8):0812004.(in Chinese)

[13] 陈建君,朱永,刘波,等.基于MEMS微镜的傅里叶变换光谱仪原理与分析[J].光谱学与光谱分析,2012,32(11):3151-3154.

CHEN J J,ZHU Y,LIU B,*et al.*. The principle and analysis of micro-Fourier transform spectrometer based on MEMS micro-mirror[J]. *Spectroscopy and Spectral Analysis*,2012,32(11):3151-3154.(in Chinese)

[14] 赵宝玮,相里斌,才啟胜,等.平行双转镜傅里叶变换光谱仪[J].光谱学与光谱分析,2015,35(11):3209-3213.

ZHAO B W,XIANG L B,CAI Q SH,*et al.*. Fourier transform spectrometer based on rotating parallel-mirror-pair[J].

Spectroscopy and Spectral Analysis, 2015, 35(11): 3209-3213. (in Chinese)

[15] 廉玉生,廖宁放,吕航,等. 一种光谱分辨率可调的新型空间调制傅里叶变换光谱仪[J]. 光谱学与光谱分析, 2014, 34(11): 3136-3140.

LIAN Y SH, LIAO N F, LV H, *et al.*. A novel spatial modulation Fourier transform spectrometer with adjustable spectral resolution[J]. *Spectroscopy and Spectral Analysis*, 2014, 34(11): 3136-3140. (in Chinese)

[16] ZHENG Y, LIANG J Q, LIANG ZH ZH. Design and fabrication of step mirrors used in space-modulated Fourier transform infrared spectrometer[J]. *Optics Express*, 2013, 21(1): 884-892.

[17] LACAN A, BRÉON F M, ROSAK A, *et al.*. A static Fourier transform spectrometer for atmospheric sounding: concept and experimental implementation[J]. *Optics Express*, 2010, 18(8): 8311-8331.

[18] 梁静秋,梁中翥,吕金光,等. 空间调制微型傅里叶变换红外光谱仪研究[J]. 中国光学, 2015, 8(2): 277-298.

LIANG J Q, LIANG ZH ZH, LV J G, *et al.*. Micro spatial modulation Fourier transform infrared spectrometer[J]. *Chinese Optics*, 2015, 8(2): 277-298. (in Chinese)

[19] CHEN CH, LIANG J Q, LIANG ZH ZH, *et al.*. Fabrication and analysis of tall-stepped mirror for use in static Fourier transform infrared spectrometer[J]. *Optics & Laser Technology*, 2015, 75: 6-12.

[20] 杨道奇,付秀华,耿似玉,等. 0.6 ~ 1.55 μm 可见/近红外超宽带增透膜的研制[J]. 中国光学, 2012, 5(3): 270-276.

YANG D Q, FU X H, GONG S Y, *et al.*. Design and fabrication of 0.6-1.55 μm visible/near infrared ultra-broad band antireflection coatings[J]. *Chinese Optics*, 2012, 5(3): 270-276. (in Chinese)

[21] FENG C, LIANG J Q, LIANG ZH ZH. Spectrum constructing with nonuniform samples using least-squares approximation by cosine polynomials[J]. *Applied Optics*, 2011, 50(34): 6377-6383.

[22] GAO J H, LIANG ZH ZH, LIANG J Q, *et al.*. Spectrum reconstruction of a spatially modulated Fourier transform spectrometer based on stepped mirrors[J]. *Applied Spectroscopy*, 2017, 71(6): 1348-1356.

作者简介:

张　敏(1989—),女,山东青岛人,博士研究生,主要从事微纳光学器件设计及制作、微光机电系统(MOEMS)等方面的研究。E-mail: 83118376@163.com

梁静秋(1962—),女,吉林长春人,博士生导师,主要从事微光机电系统(MOEMS)及红外成像光谱技术领域方面的研究。E-mail: liangjq@ciomp.ac.cn

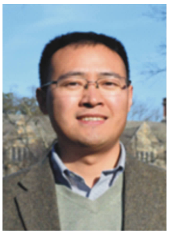

梁中翥(1978—),男,四川广安人,博士生导师,主要从事微光机电系统(MOEMS)及红外探测等方面的研究。E-mail: liangzz@ciomp.ac.cn